

## Theoretical aspects of the internal element connectivity parameterization approach for topology optimization

Gil Ho Yoon<sup>1</sup>, Yoon Young Kim<sup>2,\*</sup>,<sup>†</sup>, Matthijs Langelaar<sup>3</sup> and Fred van Keulen<sup>3</sup>

<sup>1</sup>*Department of Mechanical Engineering, Technical University of Denmark, Lyngby, Denmark*

<sup>2</sup>*Multiscale Design Center and Integrated Design & Analysis of Structures Laboratory, School of Mechanical and Aerospace Engineering, Seoul National University, Seoul, Korea*

<sup>3</sup>*Structural Optimization & Computational Mechanics Group, Department of Precision & Microsystems Engineering, Delft University of Technology, Delft, The Netherlands*

### SUMMARY

The internal element connectivity parameterization (I-ECP) method is an alternative approach to overcome numerical instabilities associated with low-stiffness element states in non-linear problems. In I-ECP, elements are connected by zero-length links while their link stiffness values are varied. Therefore, it is important to interpolate link stiffness properly to obtain stably converging results. The main objective of this work is two-fold (1) the investigation of the relationship between the link stiffness and the stiffness of a domain-discretizing patch by using a discrete model and a homogenized model and (2) the suggestion of link stiffness interpolation functions. The effects of link stiffness penalization on solution convergence are then tested with several numerical examples. The developed homogenized I-ECP model can also be used to physically interpret an intermediate design variable state. Copyright © 2008 John Wiley & Sons, Ltd.

Received 24 July 2007; Revised 3 February 2008; Accepted 7 February 2008

**KEY WORDS:** topology optimization; element connectivity parameterization; zero-length link; homogenization

### 1. INTRODUCTION

The density method [1] and the homogenization method [2] are successful in many engineering applications of the topology optimization method. However, alternative formulations [3–10] are still being developed to resolve some intrinsic numerical instabilities such as those resulting from

\*Correspondence to: Yoon Young Kim, Multiscale Design Center and Integrated Design & Analysis of Structures Laboratory, School of Mechanical and Aerospace Engineering, Seoul National University, Kwanak-Gu San 56-1, Seoul 151-742, Korea.

<sup>†</sup>E-mail: yykim@snu.ac.kr

Contract/grant sponsor: Korea Science and Technology Foundation; contract/grant number: 2006-033

low-density elements of the density method. For example, the tangent stiffness matrix loses positive definiteness in low-density elements when they experience large deformation in geometrically or materially non-linear problems. The element removal strategy proposed in [5] was effective because low-density elements are removed. A displacement-loading approach in [8] yielded satisfactory results. Recently, the element connectivity parameterization (ECP) formulation employing links to connect finite elements was introduced as an alternative method [3]. The formulation was also extended to deal with temperature under- and overshooting instability in heat transfer problems [6]. Further developments of the ECP method can be also found in [9–12]. This work is concerned with the theoretical aspects of the ECP method. The ECP method is closely related to the method developed in [4] in that domain-discretizing finite elements do not need to be rigidly connected.

Because the element-connecting link stiffness is varied in the ECP method, the effect of link stiffness on the solution behavior is different from that of the density method. Thereby, this work is focused on the investigation of the relationship between the link stiffness and the stiffness of a domain-discretizing patch. For the study, a discrete model and a homogenized model are used. The findings from the study are then used to suggest a link stiffness interpolation function that can yield distinct solid and void designs.

An overview of the ECP method will be given before theoretical investigations are carried out. To understand the way a structural layout is realized in the ECP method, consider a structural layout shown in Figure 1(a), which may appear during topology optimization iterations. The layout model by the standard density method is given in Figure 1(b), where regions of low density are represented by elements of low stiffness. The high compliance of these elements is directly related to excessive

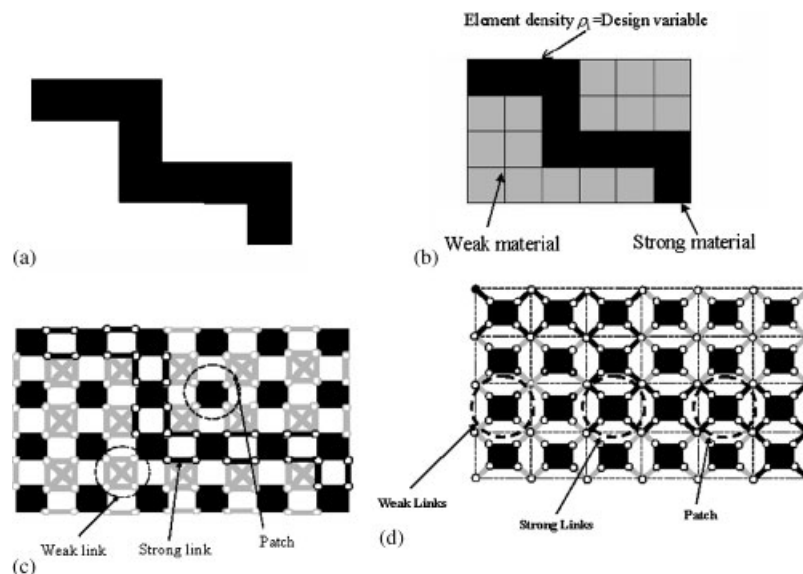


Figure 1. Comparison of different modeling techniques: (a) a given topological layout, modeling by (b) the element density method; (c) the external ECP (E-ECP) method; and (d) the internal ECP (I-ECP) method. In (c) and (d), the links are zero-length one-dimensional elastic links.

distortion and numerical instabilities [5, 7]. The models by the two versions of the ECP method are given in Figures 1(c) and (d). As illustrated in Figures 1(c) and (d), ECP does not change the material properties of the continuum element but varies the element connectivity by controlling the stiffness of the zero-length one-dimensional elastic link. Because all domain-discretizing finite elements retain their original material properties throughout the topology optimization process in the ECP approach, no numerical instability associated with low-density elements occurs. The effectiveness of the ECP method in controlling low-density-element-related numerical instabilities has been demonstrated in various situations: see [3] for optimization involving geometrical non-linearity, [9] for optimization involving material non-linearity, and [6] for optimization involving multiphysics including heat transfer. The ECP method has also been shown to be effective in the topology optimization of shape memory alloy thermal actuators involving geometrical and material non-linearities [11]. Recently, the ECP method has been extended for shell structures [12].

The apparent difference in the two ECP versions shown in Figures 1(c) and (d) lies in link location. Here, the term ‘patch’ will be used to denote the basic discretizing unit of the original design domain. In Figure 1(c), patches are the finite elements that are connected to adjacent patches by zero-length one-dimensional elastic links. These links are called external links. Note that patches do not share any node directly; they are connected through *external* links having variable stiffness. Thus, the ECP method depicted in Figure 1(c) is called the external ECP (E-ECP) method. Because patches do not share any node and all nodes are treated as independent nodes, the E-ECP formulation requires a larger number of degrees of freedom than that required by the standard density method.

The internal ECP (I-ECP) model depicted in Figure 1(d) is developed [10] to avoid the increase in the system size while maintaining the numerical instability-free characteristic of the E-ECP method. In I-ECP, every patch has *internal* links, but the degrees of freedom of the nodes defining the finite element inside a patch are eliminated at patch level by the static condensation technique. In the I-ECP formulation, thus, the number of assembled nodes determining the total system matrix is exactly the same as that required for the standard density approach. Because, in addition, computation cost for patch-level static condensation is almost negligible, I-ECP is computationally far more efficient than E-ECP. In the three-dimensional problems, the difference is even more dramatic than in the two-dimensional case [10]. Because the static condensation procedure of I-ECP can make the condensed patch stiffness vary as a non-convex function of the stiffness of the connecting link, the understanding of the stiffness behavior of the condensed patch as a function of the link stiffness is very important. This understanding will be crucial to find an appropriate link penalization form yielding clear solid and void designs at the end of topology optimization.

To investigate this stiffness behavior of the condensed patch, two approaches are considered in Section 3: the direct stiffness evaluation of a condensed finite patch and the homogenization of a microunit cell structure. In the first case, the Woodbury formula [13, 14] is used to explicitly express the stiffness matrix of the condensed patch as a function of the link stiffness. In the second case, the unit cell is composed of solid elements elastically supported along the cell boundary. Based on the investigation of the stiffness behavior, an appropriate form of the link stiffness penalization function yielding clear black-and-white images is proposed. The suggested form is to simulate solid isotropic material with penalization (SIMP)-type polynomial functions of the density approach. Section 4 subsequently deals with numerical examples that illustrate the influence and the performance of the suggested penalization scheme.

## 2. FORMULATION OF THE I-ECP METHOD

After the modeling concept of the I-ECP method is briefly presented, a procedure to construct the patch stiffness matrix by the static condensation will be briefly summarized (for detailed accounts, see [10, 15]).

Figure 2 shows a finite element representing a zero-length elastic link: an  $i$ th link connects nodes  $p$  and  $q$ . In a two-dimensional case, for example, the link is modeled by a zero-length linear spring element. If the link stiffness matrix is denoted by  $k_{i,(p,q)}^{\text{link}}$ , a single link stiffness controlling variable  $l_i^{pq}$  can be introduced

$$\begin{Bmatrix} F_x^p \\ F_y^p \\ F_x^q \\ F_y^q \end{Bmatrix} = k_{i,(p,q)}^{\text{link}} \begin{Bmatrix} u_x^p \\ u_y^p \\ u_x^q \\ u_y^q \end{Bmatrix} \quad (1)$$

$$k_{i,(p,q)}^{\text{link}} = l_i^{pq} k_{\text{nominal}}^{\text{link}} = l_i^{pq} \begin{bmatrix} 1 & 0 & -1 & 0 \\ 0 & 1 & 0 & -1 \\ -1 & 0 & 1 & 0 \\ 0 & -1 & 0 & 1 \end{bmatrix} \quad (2)$$

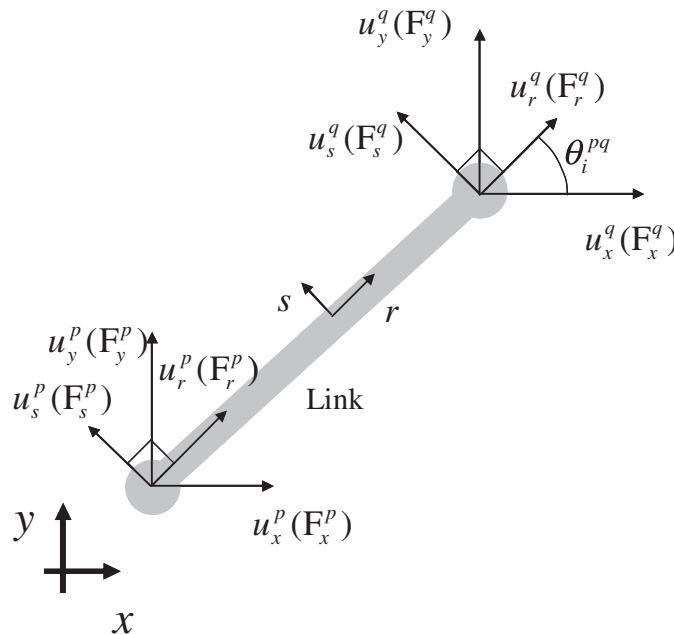


Figure 2. An  $i$ th zero-length link connecting nodes  $p$  and  $q$ . (The angle between the element coordinate system  $(r, s)$  and the global coordinate system  $(x, y)$  is denoted by  $\theta_i^{pq}$ .)

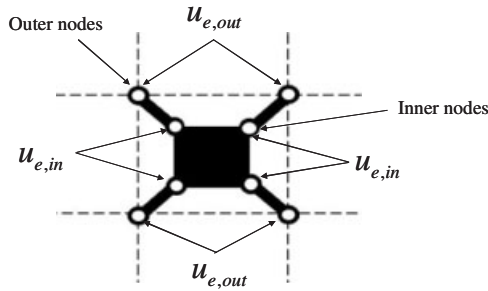


Figure 3. An  $e$ th planar rectangular patch consisting of a plane finite element and four zero-length links. The links elastically connect inner and outer nodes. The symbols  $u_{e,in}$  and  $u_{e,out}$  denote the nodal displacements of inner and outer nodes, respectively.

where  $F_{(\eta)}^{(\xi)}$  and  $u_{(\eta)}^{(\xi)}$  are the nodal force and displacement components at node  $\xi$  in the direction of  $\eta$ , respectively, and  $k_{\text{nominal}}^{\text{link}}$  denotes the nominal link stiffness. Except that the links are of zero length, links behave exactly the same as standard spring elements.

Figure 3 illustrates a rectangular patch employed in the I-ECP method in a two-dimensional setting. Every patch consists of a plane finite element and four zero-length links. In the I-ECP approach, a given design domain is discretized into patches. When the link stiffness approaches infinity, the patch discretization becomes mechanically equivalent to the discretization by standard plane finite elements. As indicated in Figure 3, the nodes lying inside and outside the patch are called the inner and outer nodes, respectively.

Although four links in a given patch can have different stiffness values for topology optimization, we simply control the four links of an  $e$ th patch by a single link stiffness variable  $l_e$  in order to reduce the total number of design variables. In other words, the following relation will be used for every patch:

$$l_e \equiv l_i^{pq} \quad (\text{for any } (p, q) \text{ combination in the } e\text{th patch}) \quad (3)$$

With Equation (3), the stiffness matrix of the  $e$ th planar patch in Figure 3 can be expressed as

$$k_{I,e} = l_e \mathbf{I}_{8 \times 8}, \quad \mathbf{I}_{8 \times 8}: \text{the } 8 \times 8 \text{ identity matrix} \quad (4)$$

$$\underbrace{\begin{bmatrix} k_{I,e} & -k_{I,e} \\ -k_{I,e} & k_{I,e} + k_e^{\text{structure}} \end{bmatrix}}_{\text{the stiffness matrix for the patch having the } e\text{th solid element}} \underbrace{\begin{Bmatrix} u_{e,out} \\ u_{e,in} \end{Bmatrix}}_{\text{the DOF of an } e\text{th patch}} = \underbrace{\begin{Bmatrix} f_{e,out} \\ f_{e,in} (=0) \end{Bmatrix}}_{\text{the applied external force}} \quad (5)$$

where  $k_e^{\text{structure}}$  is the stiffness of a solid element lying inside the  $e$ th patch. The forces applied to the outer nodes and the inner nodes are denoted by  $f_{e,out}$  and  $f_{e,in}$ , respectively. Because the external loads are applied only through the outer nodes,  $f_{e,in}$  is zero by definition.

The ECP method was shown to resolve some numerical instability problems. [3, 6, 9–11]. However, in the formulation outlined so far, it increases the total number of degrees of freedom in comparison with the standard element density method, because of the use of the additional inner

nodes. Because the increased problem dimension significantly requires the increased computational effort, we propose to employ a static condensation scheme for the degrees of freedom of the inner nodes. If  $u_{e,\text{in}}$  associated with inner nodes are condensed out in patch level [10, 15] before the system stiffness matrix is assembled, the system matrix size remains the same as the matrix size without using any link. The following equations describe the static condensation procedure:

$$u_{e,\text{in}} = (k_{I,e} + k_e^{\text{structure}})^{-1} k_{I,e} u_{e,\text{out}} \quad (6)$$

$$k_{\text{Con},e} = [k_{I,e} - k_{I,e} (k_{I,e} + k_e^{\text{structure}})^{-1} k_{I,e}] \quad (7)$$

$$k_{\text{Con},e} u_{e,\text{out}} = f_{e,\text{out}} \quad (8)$$

In deriving the patch-level condensed stiffness matrix  $k_{\text{Con},e}$ , Equation (5) was used. The final form of the system stiffness matrix  $\mathbf{K}_{\text{Con}}$  is assembled as

$$\mathbf{K}_{\text{Con}} = \sum_{e=1}^{N_p} k_{\text{Con},e} \quad (N_p: \text{the total number of patches}) \quad (9)$$

and  $\mathbf{K}_{\text{Con}}$  relates the displacement ( $\mathbf{U}_{\text{out}}$ ) and force ( $\mathbf{F}_{\text{out}}$ ) vectors of the outer nodes

$$\mathbf{K}_{\text{Con}} \mathbf{U}_{\text{out}} = \mathbf{F}_{\text{out}} \quad (10)$$

Once the static condensation scheme is applied to each patch, the size of the resulting global system matrix becomes the same as that of the density method with the same resolution without links.

### 3. STIFFNESS ANALYSIS OF THE CONDENSED I-ECP PATCH

In this section, the behavior of the condensed stiffness  $k_{\text{Con},e}$  as a function of the link stiffness variable  $l_e$  will be investigated. We begin the analysis with a discrete patch and subsequently consider a homogenized patch.

#### 3.1. Analysis using a discrete condensed patch

By using Equation (7), the behavior of the stiffness  $k_{\text{Con},e}$  as a function of  $l_e$  can be investigated. To facilitate this investigation, Equation (7) is recast into the following form:

$$k_{\text{Con},e} = k_e^{\text{structure}} \left( \mathbf{I}_{8 \times 8} + \frac{1}{l_e} k_e^{\text{structure}} \right)^{-1} \quad (11)$$

To obtain Equation (11), the following Woodbury formula [13, 14] was used:

$$(\mathbf{A} + \mathbf{U}\mathbf{V}^T)^{-1} = \mathbf{A}^{-1} - [\mathbf{A}^{-1}\mathbf{U}(\mathbf{I} + \mathbf{V}^T\mathbf{A}^{-1}\mathbf{U})^{-1}\mathbf{V}^T\mathbf{A}^{-1}] \quad (12)$$

where  $\mathbf{A}$  is a non-singular square matrix. Symbols  $\mathbf{U}$  and  $\mathbf{V}$  denote any matrices that are dimensionally compatible. By setting

$$\mathbf{A} = l_e \mathbf{I}_{8 \times 8}, \quad \mathbf{V} = \mathbf{I}_{8 \times 8}, \quad \mathbf{U} = k_e^{\text{structure}} \quad (13)$$

the matrix  $(k_{I,e} + k_e^{\text{structure}})^{-1}$ , in Equation (7), can be rewritten using Equation (12) as

$$(k_{I,e} + k_e^{\text{structure}})^{-1} = (l_e \mathbf{I}_{8 \times 8} + k_e^{\text{structure}})^{-1} = \frac{1}{l_e} \mathbf{I}_{8 \times 8} - \left[ \frac{1}{(l_e)^2} k_e^{\text{structure}} \left( \mathbf{I}_{8 \times 8} + \frac{1}{l_e} k_e^{\text{structure}} \right)^{-1} \right] \quad (14)$$

Substituting Equation (14) into Equation (7) yields Equation (11). By using Equation (11), the limiting behaviors of the condensed stiffness matrix can be analyzed

$$\lim_{l_e \rightarrow \infty} k_{\text{Con},e} = k_e^{\text{structure}} \quad \text{or} \quad \lim_{l_e \rightarrow \infty} (k_{\text{Con},e})^{-1} = (k_e^{\text{structure}})^{-1} \quad (15)$$

$$\lim_{l_e \rightarrow 0} k_{\text{Con},e} = \mathbf{0} \quad \text{or} \quad \lim_{l_e \rightarrow 0} (k_{\text{Con},e})^{-1} = \infty \mathbf{I}_{8 \times 8} \quad (16)$$

Equations (15) and (16) clearly show that the condensed system matrix  $k_{\text{Con},e}$  reduces to the stiffness matrix of the original material or a void in either limit.

Now let us investigate how the stiffness of the condensed patch varies as the function of the link stiffness variable  $l_e$ . Appropriate values for upper ( $l_{\max}$ ) and lower ( $l_{\min}$ ) bounds of link stiffness should also be determined during the investigation:

$$l_{\min} < l_e < l_{\max} \quad (17)$$

As a means of examining the behavior of the condensed matrix  $k_{\text{Con},e}$ , the following norm of the condensed matrix  $k_{\text{Con},e}$  normalized with respect to the stiffness matrix  $k_e^{\text{structure}}$  of a discretizing element will be used:

$$\frac{\|k_{\text{Con},e}(l_e)\|}{\|k_e^{\text{structure}}\|} = \|(\mathbf{I}_{8 \times 8} + 1/l_e k_e^{\text{structure}})^{-1}\| \quad (18)$$

where  $\|\cdot\|$  denotes the largest singular value.

As a benchmark case, consider a single patch in the I-ECP method in Figure 3 for a linear isotropic material (Young's modulus  $E = 1.0 \text{ Pa}$ , the Poisson ratio  $\nu = 0.3$ ). The norm defined in (18) is plotted in Figure 4 and the difference  $\|k_{\text{Con},e}(l_e)\|/\|k_e^{\text{structure}}\|$  is calculated in Table I for varying values of the patch link stiffness  $l_e$ . As predicted by Equations (15) and (16), the condensed system matrix approaches the original matrix  $k_e^{\text{structure}}$  for a large  $l_e$  and a zero matrix for a small  $l_e$ . In Table I and Figure 4,  $k_{\text{diagonal}}^{\text{structure}}$  denotes the mean value of the diagonal terms in  $k_e^{\text{structure}}$ .<sup>‡</sup> For instance, the diagonal terms of the four-node plane element are given by [15]

$$k_e^{\text{structure}}(i, i) = \frac{tE}{(1-\nu^2)} \left( \frac{b}{3a} + \frac{1}{6} \frac{a}{b} (1-\nu) \right) \quad (i = 1, 3, 5, 7)$$

$$k_e^{\text{structure}}(i, i) = \frac{tE}{(1-\nu^2)} \left( \frac{a}{3b} + \frac{1}{6} \frac{b}{a} (1-\nu) \right) \quad (i = 2, 4, 6, 8)$$

<sup>‡</sup>The quantity  $l_e$  may be normalized with respect to Young's modulus because the expression of  $k_{\text{diagonal}}^{\text{structure}}$  is somewhat complicated. However,  $k_{\text{diagonal}}^{\text{structure}}$  appears to be more convenient as proper values selected for  $l_{\max}$  and  $l_{\min}$  relative to  $k_{\text{diagonal}}^{\text{structure}}$  in one problem can be used for other problems such as shell problems.

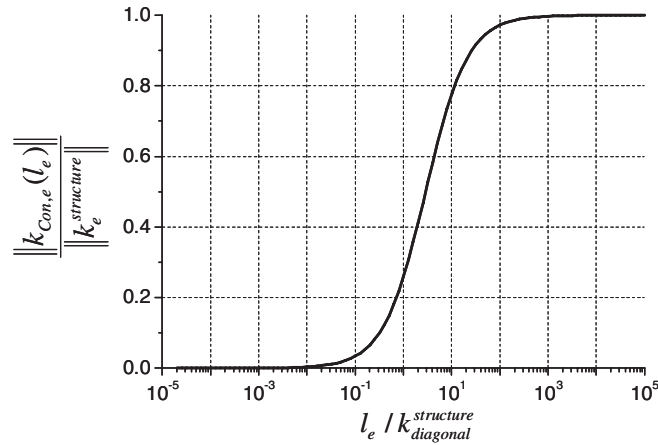


Figure 4. The matrix norm  $\|k_{\text{Con},e}(l_e)\|/\|k_e^{\text{structure}}\|$  as a function of the link stiffness  $l_e$ .

Table I. The difference in the matrix norm.

$l_e/k_{\text{diagonal}}^{\text{structure}}$	$\ k_{\text{Con},e}(l_e)\ /\ k_e^{\text{structure}}\ $
$10^{-5}$	$3.4615 \times 10^{-6}$
$10^{-3}$	$3.4603 \times 10^{-4}$
$10^0$	0.2571
$10^3$	0.9971
$10^5$	1.0000

where  $E$  and  $\nu$  are Young's modulus and the Poisson ratio. The width, height, and thickness of the element are denoted by  $a$ ,  $b$ , and  $t$ , respectively. The results in Figure 4 and Table I suggest that the ratio  $l_e$  to  $k_{\text{diagonal}}^{\text{structure}}$  should be sufficiently small (say,  $O(10^{-3})$ ) to simulate a void and sufficiently large (say,  $O(10^3)$ ) to simulate a solid. The estimation of  $k_e^{\text{structure}}$  is given only for a rectangular mesh, but the finding that the use of  $l_e/k_e^{\text{structure}} = O(10^3)$  is useful for general meshes is demonstrated for triangular meshes in [12].

Note that the matrix norm in Figure 4 is not a simple convex function of  $l_e$ . Therefore, a procedure to develop a convex penalization function, similar to a SIMP function, will be discussed later in more details.

At this point, it is necessary to check whether small  $l_e$  values used to simulate voids cause any numerical difficulty especially in geometrically non-linear problems. To this end, the analysis of a geometrically non-linear cantilever beam is considered in Figure 6. The original model and the deformed shape are shown in Figure 5(a) whereas those by the standard density approach and I-ECP approach are shown in Figures 5(b) and (c), respectively. Note that the void region is represented by the region of low-density elements in Figure 5(b) and by the region of one-dimensional links in Figure 5(c), respectively. The convergence histories of the Newton–Raphson

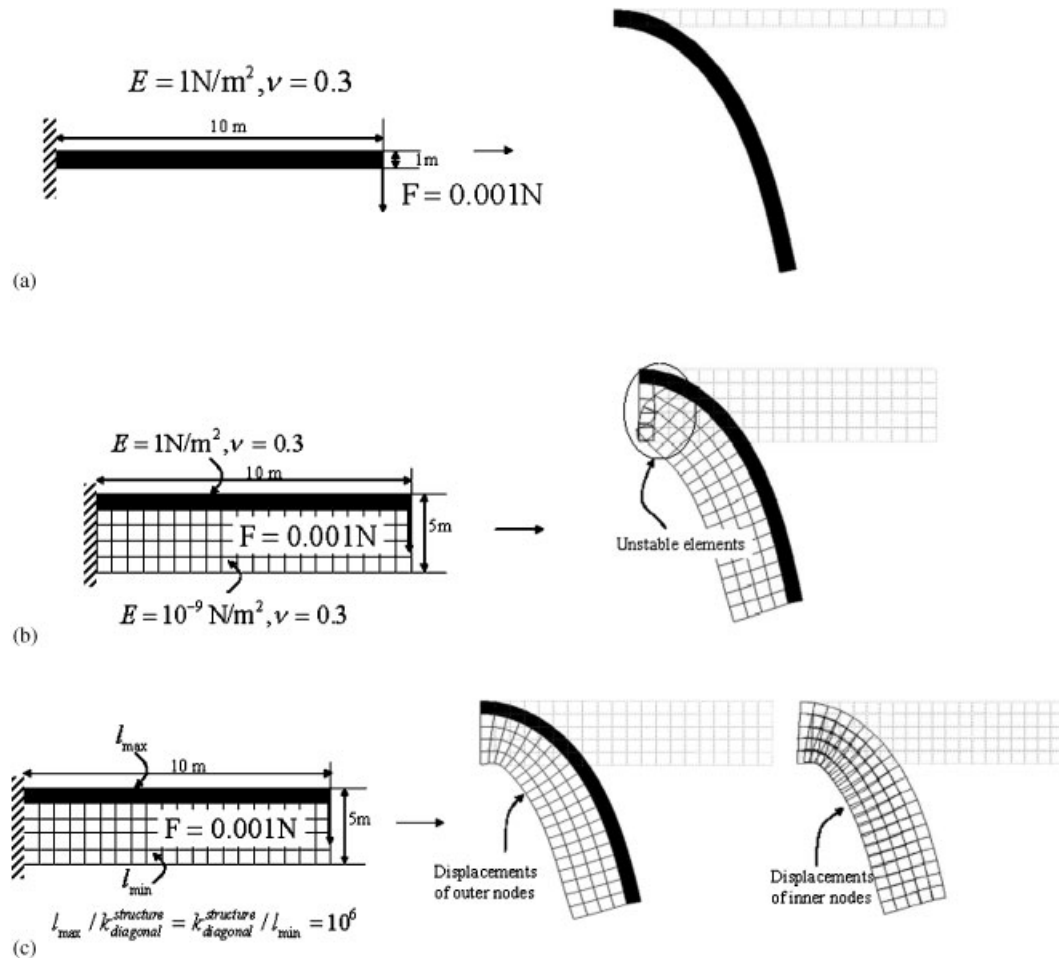


Figure 5. Numerical stability test of the I-ECP method for a geometrically non-linear structure when: (a) an original model; (b) a model used by a density method; and (c) a model used by the I-ECP method are used.

method in the three modeling approaches are compared in Figure 6. Because no unstable element appears in the I-ECP method, the solution convergence is stable in Figure 6(c). For more details about the stable behavior of I-ECP in non-linear problems, see Reference [10].

### 3.2. The stiffness behavior of an elastically supported microunit cell

Figure 7(b) shows a periodic elastically supported microunit cell equivalent to an I-ECP patch in Figure 7(a). The unit cell in Figure 7(b) represents an elastic cell supported by elastic foundations along its sides. By correlating the I-ECP patch and the microstructure, one may interpret the I-ECP model as a discrete version of a continuum structure with varying elastic foundation stiffness.

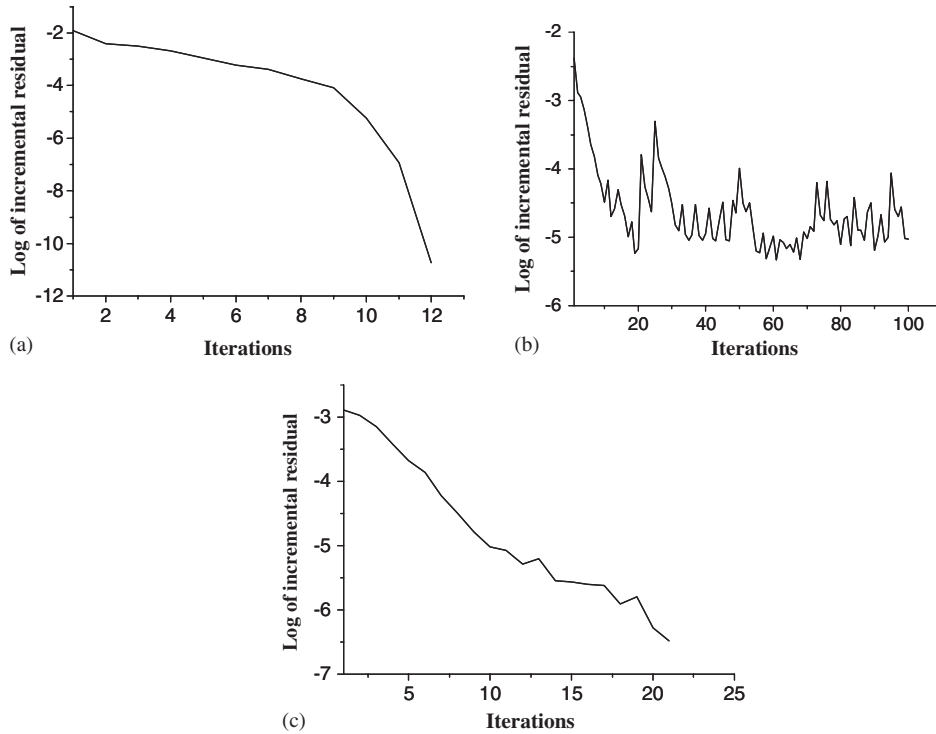


Figure 6. Convergence histories of the Newton–Raphson method using: (a) the original model; (b) the I-ECP model; and (c) the density model.

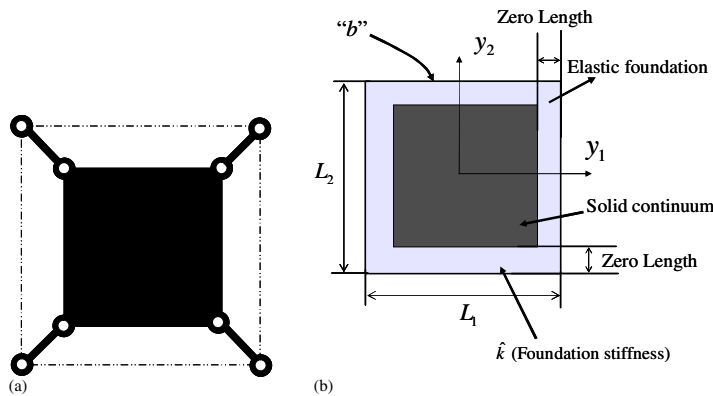


Figure 7. Comparison of two equivalent models: (a) I-ECP patch and (b) elastically supported continuum unit cell. (Symbols  $y_i$  denote the microscale coordinates.)

Consequently, a physical model corresponding to intermediate link stiffness can be also envisioned. To evaluate the stiffness of the microunit cell in Figure 7(b), the homogenization technique (see, e.g. [16]) will be employed.

In Figure 7(b), the periodic unit cell is defined on

$$Y = \left[ \frac{-L_1}{2}, \frac{L_1}{2} \right] \times \left[ \frac{-L_2}{2}, \frac{L_2}{2} \right]$$

and  $y_i$  denote the microscopic coordinates. The elastic foundation occupies no area. The horizontal and vertical foundation stiffnesses are denoted by  $\hat{k}$ . For a weak formulation required for the homogenization procedure, let us introduce  $v_i$  (the virtual displacement of the solid continuum) and  ${}_b v_i$  (the virtual displacement along the cell boundary at 'b'). Then, the weak form of the microscale equilibrium equation for characteristic displacements  $\chi_p^{kl}$  of the solid and  ${}_b \chi_p^{kl}$  of the boundary can be expressed as

$$\begin{aligned} & \int_Y C_{ijkl} \frac{\partial \chi_p^{kl}}{\partial y_q} \frac{\partial v_i}{\partial y_j} dY \\ & + \int_{-L_1/2}^{L_1/2} \hat{k} (\chi_i^{kl} - {}_b \chi_i^{kl}) (v_j - {}_b v_j) dy_1 \Big|_{y_2=-L_2/2} - \int_{-L_1/2}^{L_1/2} \hat{k} (\chi_i^{kl} - {}_b \chi_i^{kl}) (v_j - {}_b v_j) dy_1 \Big|_{y_2=L_2/2} \\ & + \int_{-L_2/2}^{L_2/2} \hat{k} (\chi_i^{kl} - {}_b \chi_i^{kl}) (v_j - {}_b v_j) dy_2 \Big|_{y_1=-L_1/2} - \int_{-L_2/2}^{L_2/2} \hat{k} (\chi_i^{kl} - {}_b \chi_i^{kl}) (v_j - {}_b v_j) dy_2 \Big|_{y_1=L_1/2} \\ & = \int_Y C_{ijkl} \frac{\partial v_i}{\partial y_j} dY \end{aligned} \quad (19)$$

where  $C_{ijkl}$  denotes the elastic coefficients of the solid in the unit cell.

Once the solution  $\chi_p^{kl}$  of (19) is obtained, the homogenized elasticity coefficients  $C_{ijkl}^H$  are calculated as

$$C_{ijkl}^H = \frac{1}{|Y|} \int_Y C_{ijkl} - C_{ijpq} \frac{\partial \chi_p^{kl}}{\partial y_q} dY \quad (20)$$

where  $|Y| = L_1 L_2 = L^2$  if  $L_1 = L_2 = L$ . Note that  ${}_b \chi_p^{kl}$  does not contribute to the homogenized elasticity coefficient because the elastic foundation occupies no area. However, the presence of  $\hat{k}$  and the non-vanishing values of  ${}_b \chi_p^{kl}$  do affect the solution  $\chi_p^{kl}$  in Equation (19).

Figure 8 illustrates the unit cell discretized by finite elements to solve Equation (19). If the number of continuum finite elements (such as bilinear plane elements) is  $n_e \times n_e$ , each side is supported by  $(n_e + 1)$  one-dimensional zero-length springs. For  $L_1 = L_2 = L$ , the spring stiffness becomes

$$k = \frac{\hat{k}L}{n_e} \quad (21a)$$

but the stiffness of springs on the corners should be evaluated as

$$k = \frac{1}{2} \frac{\hat{k}L}{n_e} \quad (21b)$$

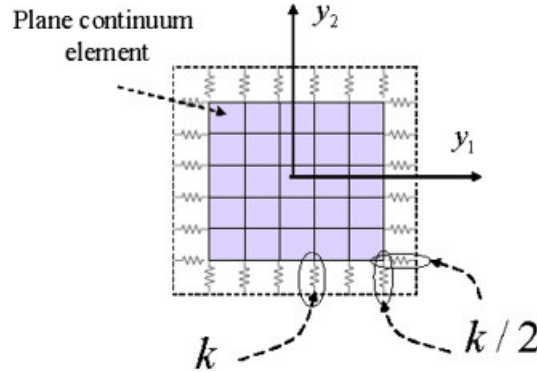


Figure 8. The finite element discretization of a unit cell in Figure 7(b).

If the elastic foundation stiffness is set to be

$$\hat{k} = \frac{l_e}{L} \quad (22)$$

and  $L$  is chosen to be the length of an I-ECP patch, the two models in Figure 7 become equivalent from a mechanical point of view.

The boundary conditions for the finite element model in Figure 8 can be determined by considering solution periodicity and the symmetry of loading for  $\chi_p^{(11)}$  and  $\chi_p^{(22)}$ . An antisymmetry condition is applied to  $\chi_p^{(12)}$ . The following boundary conditions are used to solve Equation (19):

- (1) For  $\chi_p^{kl}$  with  $(kl) = (11)$  or  $(22)$

$${}_b\chi_1^{(kl)} = 0 \text{ for } y_1 = \pm L/2, \quad {}_b\chi_2^{(kl)} = 0 \text{ for } y_2 = \pm L/2$$

- (2) For  $\chi_p^{kl}$  with  $(kl) = (12)$

$${}_b\chi_2^{(kl)} = 0 \text{ for } y_1 = \pm L/2, \quad {}_b\chi_1^{(kl)} = 0 \text{ for } y_2 = \pm L/2$$

Once the solution  $\chi_p^{kl}$  is obtained, the homogenized elastic coefficients  $C_{ijkl}^H$  are calculated from Equation (20). For the numerical calculation of  $C_{ijkl}^H$ , four-node bilinear finite elements ( $Q4$  elements) were used to discretize the solid area in Figure 8.

Figures 9(a–c) show the deformed shape of the unit cell due to  $\chi_p^{11}$ ,  $\chi_p^{22}$ , and  $\chi_p^{12}$ , respectively. Using  $\chi_p^{kl}$  obtained in Figure 9, the norms of the homogenized elastic constants  $C_{ijkl}^H$  are plotted in Figure 10 as a function of  $\hat{k}L/k_{\text{diagonal}}^{\text{structure}}$ . The comparison of Figures 4 and 10 shows that the non-convex behavior of the norms results from the presence of the elastic foundation stiffness. Using (22), one can identify an elastically supported microstructure corresponding to an intermediate value of  $l_e$ . In this way, a physical interpretation can be given to the I-ECP layout modeling approach.

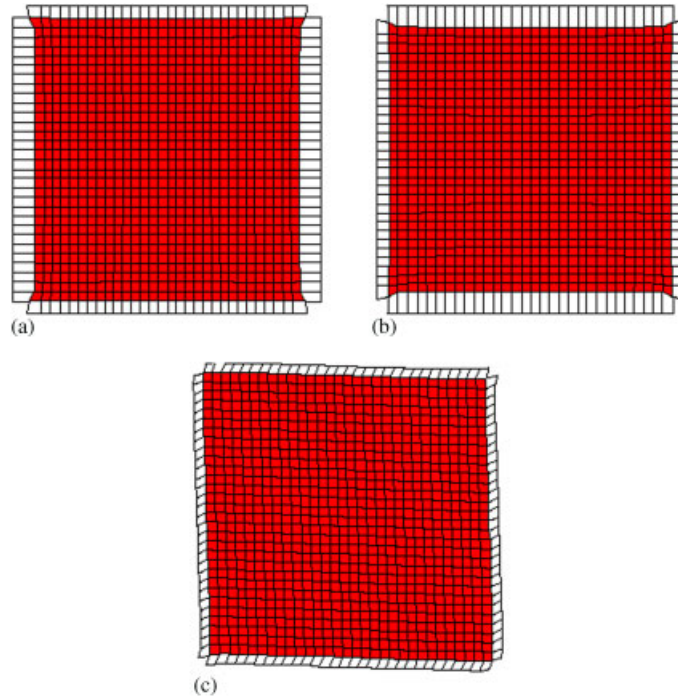


Figure 9. The deformed unit cells due to: (a)  $\chi_p^{(11)}$ ; (b)  $\chi_p^{(22)}$ ; and (c)  $\chi_p^{(12)}$  ( $p=1, 2$ ).

### 3.3. Link stiffness interpolation

To find a proper link stiffness interpolation function, the following observations are made from the analysis of Sections 3.1 and 3.2.

- (1) The relationship between the link stiffness  $l_e$  and the condensed patch stiffness ( $\|k_{\text{Con},e}\|$ ) is not a convex function.
- (2) Equivalently, the relationship between the foundation stiffness  $\hat{k}$  and the homogenized elastic constant ( $\|C_{ijkl}^H\|$ ) is not a convex function.

Therefore, if  $l_e$  is used as the design variable  $\gamma_e$  with simple polynomial interpolation,  $k_{\text{Con},e}$  cannot be properly penalized. Figure 11 shows the behavior of  $\|k_{\text{Con},e}\|$  (Young's modulus  $E=1$  and the Poisson ratio  $\nu=0.3$ ) as a function  $\gamma_e$  when the simple polynomial interpolation function is used

$$\text{Polynomial interpolation: } l_e = (l_{\max} - l_{\min})\gamma_e^n + l_{\min} \quad (23)$$

with

$$0 = \gamma_{\min} \leq \gamma_e \leq \gamma_{\max} = 1 \quad (24)$$

where  $n$  is the penalty exponent. The I-ECP patch mass  $m_e$  will be interpolated as

$$m_e = m_0 \gamma_e \quad (25)$$

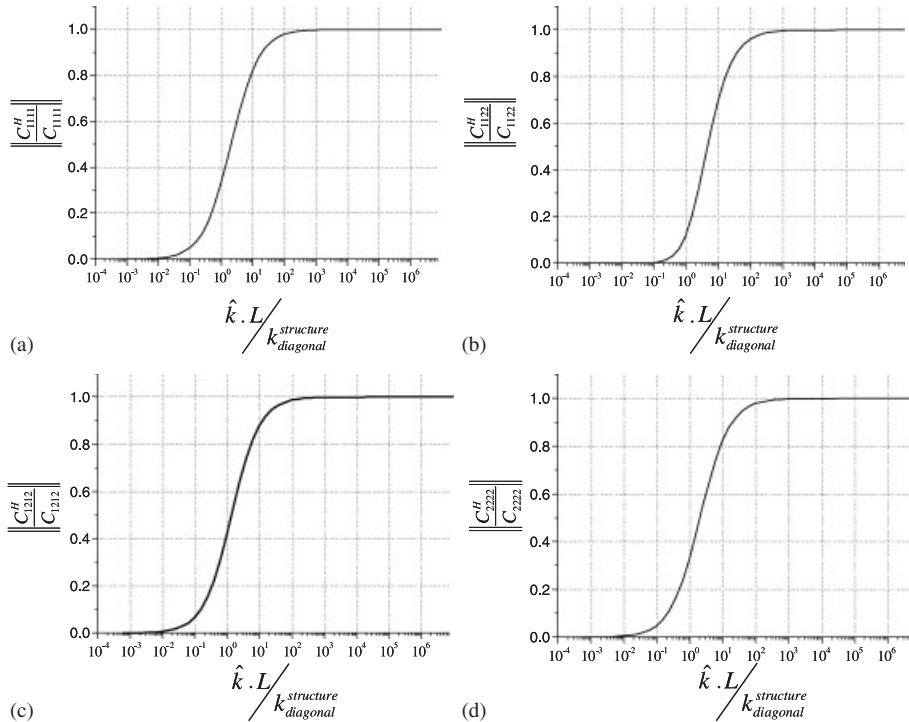


Figure 10. The norms of the homogenized elastic coefficients of an elastically supported unit cell. ( $\hat{k}$ : foundation stiffness;  $L$ : cell length;  $k_{diagonal}^{structure}$ : the largest diagonal stiffness of the  $Q4$  element modeling the solid of the unit cell). Note that  $\hat{k}L = l_e$ .

when  $m_0$  is the mass of the solid finite element in the patch. Structural layouts will be rendered based on (25).

Figure 11 shows that the polynomial interpolation properly penalizes in Region A where the design variable takes on small values ( $n > 1$ ). However, there exists a region marked by Region B where  $\|k_{Con,e}\| / \|k_e^{structure}\| > \gamma_e$ . Even with very large values of  $n$  such as  $n=20$  or  $40$ , the region for which  $\|k_{Con,e}\| / \|k_e^{structure}\| > \gamma_e$  cannot be avoided. Thus, typical compliance minimization problems tend to favor intermediate design variables lying in Region B. As a result, it will be difficult to obtain distinct solid and void results unless an additional condition is introduced. This motivated us to consider other interpolation functions different from Equation (23). Among them, the following interpolation function is considered:

$$l_e = \alpha \frac{\gamma^n}{1 + (1 - \gamma^n) \frac{\alpha}{k_{diagonal}^{structure} \times m}} + \beta \quad (26)$$

where  $m$  is the number of degrees of freedom per node (in the present plane problem case,  $m = 2$ ) and

$$\alpha = l_{\max} - l_{\min}, \quad \beta = l_{\min} \quad (27)$$

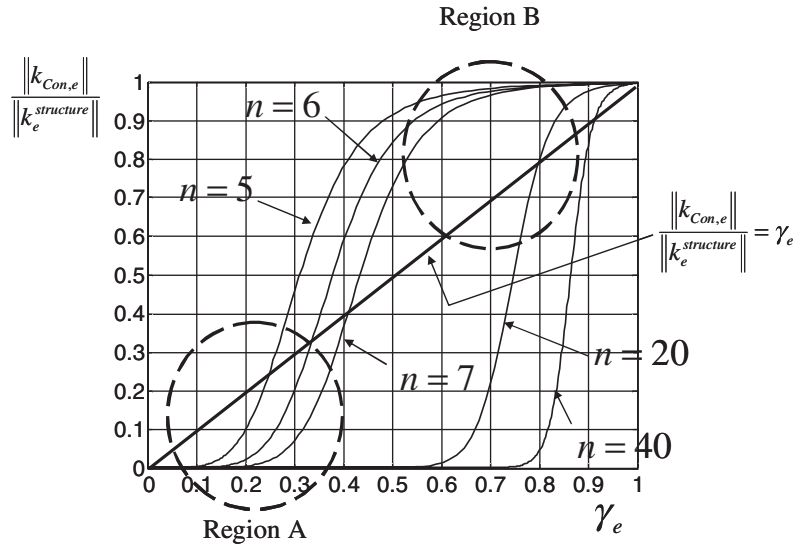


Figure 11. The behavior of the stiffness norm for varying powers of the polynomial interpolation in Equation (23) ( $l_{\max} = 10^3 \times k_{\text{diagonal}}^{\text{structure}}$ ,  $l_{\min} = 10^{-3} \times k_{\text{diagonal}}^{\text{structure}}$ ).

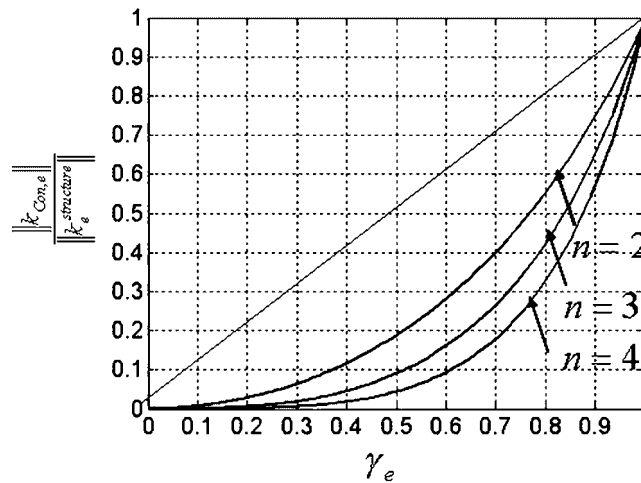


Figure 12. The behavior of the stiffness norm for powers of the polynomial interpolation in Equation (26).

The formula in Equation (26) turns out to be a rational function as suggested in [17], although the motivation to use the interpolation equation (26) is somewhat different.

To investigate the behavior of the condensed stiffness matrix  $k_{\text{Con},e}$ , the values of the penalty exponent  $n$  are varied. The norm of  $k_{\text{Con},e}$  in Figure 12 is plotted as the function of the design variable  $\gamma_e$ . When Equation (26) is used, the norm  $\|k_{\text{Con},e}\|/\|k_e^{\text{structure}}\|$  lies below the linear curve;

the  $\|k_{\text{Con},e}\|-\gamma_e$  relationship in Figure 10 now exhibits proper penalization necessary to yield distinct solid and void layouts.

#### 4. INFLUENCE OF THE I-ECP LINK STIFFNESS PENALIZATION ON OPTIMIZATION CONVERGENCE

In this section, the effectiveness of the I-ECP method with the penalization function in Equation (26) is demonstrated using simple examples. In particular, the effects of  $l_{\text{max}}$ ,  $l_{\text{min}}$ , and  $n$  on the convergence of the topology optimization process are studied. The numerical examples are

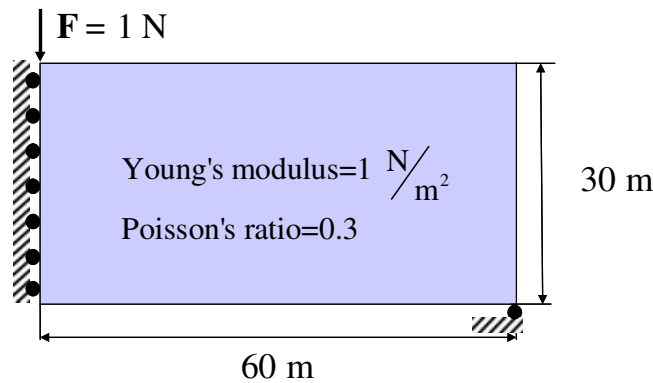


Figure 13. A compliance minimization problem under 30% mass constraint.

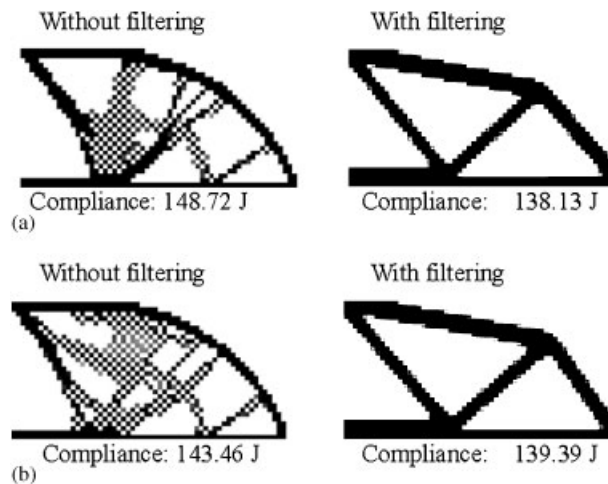


Figure 14. Comparison of the results by the standard density method (MATLAB code in Reference [18]) and the I-ECP method (MATLAB code in Appendix A). Results by (a) the density-based approach and (b) the I-ECP approach.

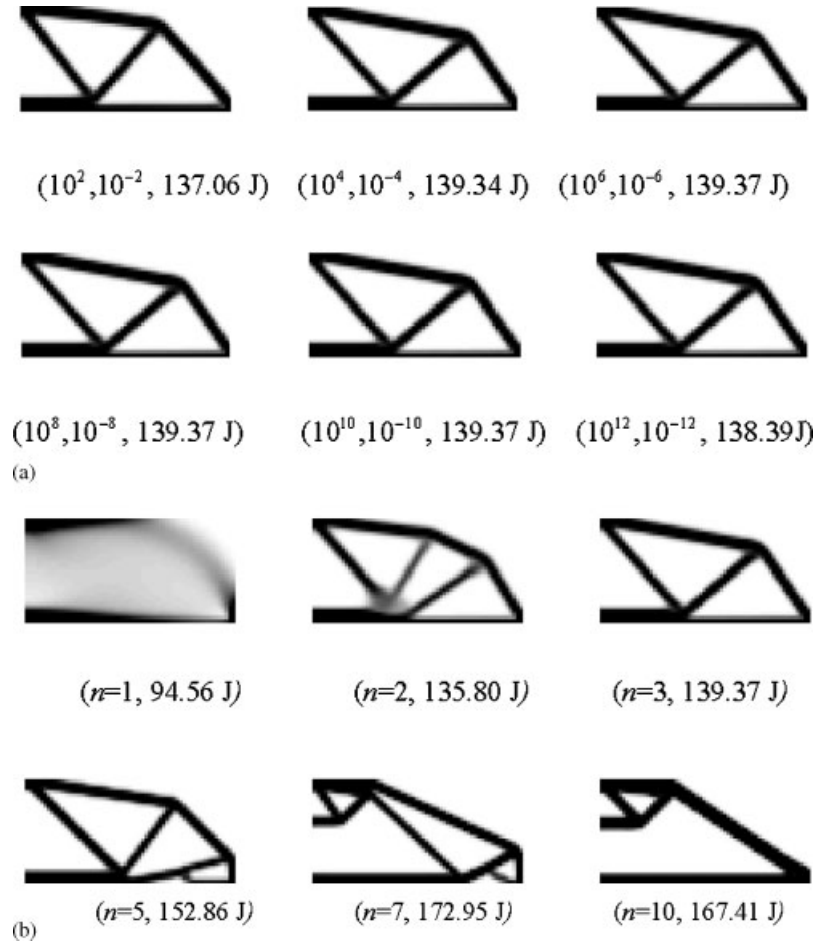


Figure 15. (a) The effects of  $l_{\max}$  and  $l_{\min}$  (The values in parentheses denote  $l_{\max}/k_{\text{diagonal}}^{\text{structure}}$ ,  $l_{\min}/k_{\text{diagonal}}^{\text{structure}}$ , and the objective function value) and (b) the effects of  $n$  on the solution convergence for  $l_{\max}/k_{\text{diagonal}}^{\text{structure}} = k_{\text{diagonal}}^{\text{structure}}/l_{\min} = 10^9$  (The values in parentheses denote  $n$  and the objective function value).

limited to linear two-dimensional problems. For a detailed discussion of application of I-ECP to the topology optimization of three-dimensional geometrically non-linear structures, see [10].

To demonstrate the effects of the involved parameters on the solution convergence, a simple compliance minimization problem shown in Figure 13 is considered. Because the detailed strategy and the procedure for these types of problems have already been given in [10], no problem-solving procedure will be repeated here. Instead, an I-ECP MATLAB implementation for compliance minimization is included in Appendix A. The design domain is discretized into  $60 \times 30$  patches. In solving the problem,  $l_{\max}/k_{\text{diagonal}}^{\text{structure}} = 1.0 \times 10^9$  and  $l_{\min}/k_{\text{diagonal}}^{\text{structure}} = 1.0 \times 10^{-9}$  are used. For stiffness interpolation, Equation (26) was used with  $n = 3$ .

Before checking the effects of the involved parameters, the performance of the I-ECP method is tested against that of the standard density method. To this end, Figure 14 compares the I-ECP









	Density method with SIMP	ECP
$\nu = 0.499$	 Compliance: 139.06 J	 Compliance: 138.32 J
$\nu = 0.0$	 Compliance: 139.29 J	 Compliance: 138.90 J
$\nu = 0.3$	 Compliance: 138.13 J	 Compliance: 139.37 J
$\nu = -0.5$	 Compliance: 136.97 J	 Compliance: 134.61 J

Figure 16. The effects of the Poisson ratio.

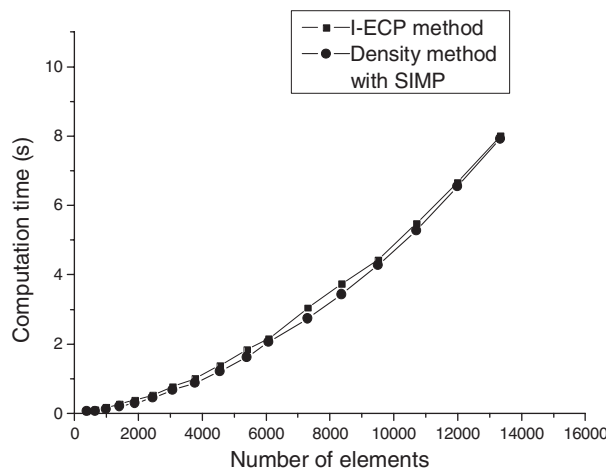


Figure 17. CPU time for the calculation of nodal displacements and the sensitivity values per an iteration by the I-ECP and the density methods with SIMP.

results with those obtained by the code given in [18]. As demonstrated in [19], checkerboards cannot be avoided unless locking-free finite elements such as non-conforming finite elements are used. Because standard four-node displacement elements are used in this work, the sensitivity filter developed and implemented by Sigmund [18] is used to control checkerboards. (The radius of the used filter is 1.5.)

Figure 15 shows the effects of the involved parameters ( $l_{\max}$ ,  $l_{\min}$ ,  $n$ ) on the solution convergence of the I-ECP method. As long as the penalty exponent is moderately large (say  $n = 3.0$ ), the effects of  $l_{\max}$  and  $l_{\min}$  are not so significant; see the layout configurations and the final compliance values. However, too large values of  $n$  should be avoided as they tend to yield local optima. The robustness with respect to the values of the Poisson ratio is demonstrated in Figure 16 and compared with that by the density method using SIMP.

Finally, the computation times by the I-ECP method and by the standard finite element without any link are compared in Figure 17. As the static condensation in Equation (7) requires the inversion of element stiffness matrices, additional computation cost may be a concern. However, the cost is marginal as demonstrated in Figure 17 because the dominant cost comes from the matrix decomposition of the global system matrix.

Because this investigation is mainly considered with the theoretical aspects of the I-ECP method and determination of an adequate relationship between the link stiffness and the design variables, no topology optimization involving non-linear analysis was considered. See [3, 9–11] for the applications of the I-ECP method in non-linear problems.

## 5. CONCLUSIONS

This investigation was focused on theoretical aspects of the I-ECP method, particularly on the behavior of the stiffness matrix of an I-ECP patch as a function of the link stiffness. The I-ECP method was developed for computationally efficient and trouble-free topology optimization for geometrically and materially non-linear and thermal design problems. The first part of this study showed that the stiffness matrix of a patch used in the I-ECP method behaves as a non-convex function of the elastic link stiffness. However, if the link stiffness is interpolated by a rational function of a design variable, the patch stiffness matrix can become a convex function of the design variable. Subsequently, the resulting convergence properties of the penalized I-ECP method then become very similar to those of the density-based SIMP results, in the linear case. It was also shown that the I-ECP method is equivalent to using homogenized microcells made of elastically supported continuum solids. Thereby, a microstructure can be associated with an I-ECP patch having an intermediate design variable.

## APPENDIX A: I-ECP MATLAB IMPLEMENTATION

An MATLAB implementation of the I-ECP method to solve the compliance minimization problem is presented below. The following code is modified from the MATLAB code in Reference [18]. Modifications with respect to the original code are identified by underlines.

```

1.  %A MATLAB CODE FOR I-ECP IMPLEMENTATION
2.  function IECP(nelx, nely, volfrac, penal, rmin, lmax, lmin)
3.  % INITIALIZE
4.  x(1:nely, 1:nelx) = volfrac;
5.  loop = 0;
6.  change = 1.;
7.  % START ITERATION
8.  while change > 0.01

```

```

9.   loop=loop+1;
10.  xold=x;
11.  % FE-ANALYSIS
12.  [U, c]=FE(nelx, nely, x, penal, lmax, lmin);
13.  % OBJECTIVE FUNCTION AND SENSITIVITY ANALYSIS
14.  [KE]=lk; sdiag=sum(diag(KE))/8.0*2;
15.  for ely=1:nely
16.  for elx=1:nelx
17.  n1=(nely+1)*(elx-1)+ely;
18.  n2=(nely+1)*elx+ely;
19.  Uout=U([2*n1-1; 2*n1; 2*n2-1; 2*n2; 2*n2+1; 2*n2+2; 2*n1+1; 2*n1+2], 1);
20.  lp=(lmax-lmin)*x(ely, elx)^penal/(1+(1-x(ely, elx)^penal)*(lmax-lmin)/sdiag);
21.  Uin=(lp+lmin)*inv((lp+lmin)*eye(8, 8)+KE)*Uout;
22.  dc(ely, elx)=-penal/x(ely, elx)*(lp+lp^2/sdiag)*(Uout-Uin)^(Uout-Uin);
23.  end
24.  end
25.  % FILTERING OF SENSITIVITIES
26.  [dc]=check(nelx, nely, rmin, x, dc);
27.  % DESIGN UPDATE BY THE OPTIMALITY CRITERIA METHOD
28.  [x]=OC(nelx, nely, x, volfrac, dc);
29.  % PRINT RESULTS
30.  change=max(max(abs(x-xold)));
31.  disp([' It.: ' sprintf('%4i',loop) ' Obj.: ' sprintf('%10.4f',c)...
32.  ' Vol.: ' sprintf('%6.3f',sum(sum(x))/(nelx*nely))...
33.  ' ch.: ' sprintf('%6.3f',change)])
34.  % PLOT DENSITIES
35.  colormap(gray); imagesc(-x); axis equal; axis tight; axis off; pause(1e-6);
36.  end
37.  %%%OPTIMALITY CRITERIA UPDATE %%%
38.  function [xnew]=OC(nelx, nely, x, volfrac, dc)
39.  l1=0; l2=1000000000; move=0.1;
40.  while (l2-l1>1e-6)
41.  lmid=0.5*(l2+l1);
42.  xnew=max(1.0E-8, max(x-move, min(1., min(x+move, x.*(-dc./lmid).^0.5))));
43.  if sum(sum(xnew))-volfrac*nelx*nely>0;
44.  l1=lmid;
45.  else
46.  l2=lmid;
47.  end
48.  end
49.  %%%MESH-INDEPENDENCY FILTER %%%
50.  function [dcn]=check(nelx, nely, rmin, x, dc)
51.  dcn=zeros(nely, nelx);
52.  for i=1:nelx
53.  for j=1:nely
54.  sum=0.0;

```

```

55.   for k = max(i - floor(rmin), 1) : min(i + floor(rmin), nelx)
56.   for l = max(j - floor(rmin), 1) : min(j + floor(rmin), nely)
57.   fac = rmin - sqrt((i - k)^2 + (j - l)^2);
58.   sum = sum + max(0, fac);
59.   dcn(j, i) = dcn(j, i) + max(0, fac) * x(l, k) * dc(l, k);
60.   end
61.   end
62.   dcn(j, i) = dcn(j, i) / (x(j, i) * sum);
63.   end
64.   end
65.   %%%FE-ANALYSIS %%%
66.   function [U, c] = FE(nelx, nely, x, penal, lmax, lmin)
67.   [KE] = lk; sdiag = sum(diag(KE)) / 8.0^2;
68.   K = sparse(2 * (nelx + 1) * (nely + 1), 2 * (nelx + 1) * (nely + 1));
69.   F = sparse(2 * (nelx + 1) * (nely + 1), 1); U = zeros(2 * (nelx + 1) * (nely + 1), 1);
70.   for elx = 1 : nelx
71.   for ely = 1 : nely
72.   n1 = (nely + 1) * (elx - 1) + ely; n2 = (nely + 1) * elx + ely;
73.   edof = [2 * n1 - 1; 2 * n1; 2 * n2 - 1; 2 * n2; 2 * n2 + 1; 2 * n2 + 2; 2 * n1 + 1; 2 * n1 + 2];
74.   K(edof, edof) = K(edof, edof) + KE * inv(eye(8) + 1 / ((lmax - lmin) * x(ely, elx) ^ penal) / (1 +
(1 - x(ely, elx) ^ penal) * (lmax - lmin) / sdiag) + lmin) * KE);
75.   end
76.   end
77.   % DEFINE LOADS AND SUPPORTS (HALF MBB-BEAM)
78.   F(2, 1) = -1;
79.   fixeddofs = union([1 : 2 * (nely + 1)], [2 * (nelx + 1) * (nely + 1)]);
80.   alldofs = [1 : 2 * (nely + 1) * (nelx + 1)];
81.   freedofs = setdiff(alldofs, fixeddofs);
82.   % SOLVING
83.   U(freedofs, :) = K(freedofs, freedofs) \ F(freedofs, :);
84.   U(fixeddofs, :) = 0;
85.   c = U' * F;
86.   %%%ELEMENT STIFFNESS MATRIX %%%
87.   function [KE] = lk
88.   E = 1.;
89.   nu = 0.3;
90.   k = [1/2 - nu/6   1/8 + nu/8 - 1/4 - nu/12 - 1/8 + 3*nu/8...
91.   -1/4 + nu/12 - 1/8 - nu/8   nu/6   1/8 - 3*nu/8];
92.   KE = E / (1 - nu^2) * [k(1) k(2) k(3) k(4) k(5) k(6) k(7) k(8)
93.   k(2) k(1) k(8) k(7) k(6) k(5) k(4) k(3)
94.   k(3) k(8) k(1) k(6) k(7) k(4) k(5) k(2)
95.   k(4) k(7) k(6) k(1) k(8) k(3) k(2) k(5)
96.   k(5) k(6) k(7) k(8) k(1) k(2) k(3) k(4)
97.   k(6) k(5) k(4) k(3) k(2) k(1) k(8) k(7)
98.   k(7) k(4) k(5) k(2) k(3) k(8) k(1) k(6)
99.   k(8) k(3) k(2) k(5) k(4) k(7) k(6) k(1)];

```

The design variables  $\gamma$  are denoted by 'x' in the above I-ECP code. It can be seen that only small modifications are required to modify a density-based topology optimization implementation into an I-ECP-based one. Because I-ECP requires  $k_{\text{Con},e}$  in Equations (7) and (14), the following line must be included in the code:

```
74. K(edof, edof) = K(edof, edof) + KE*inv(eye(8) + 1/((lmax - lmin)*x(ely, elx)^penal/(1 +
    (1 - x(ely, elx)^penal)*(lmax - lmin)/sdiag) + lmin)*KE);
```

The following three lines are used to compute the nodal displacements of inner and outer nodes, which are denoted by Uout and Uin, respectively.

```
19. Uout = U([2*n1 - 1; 2*n1; 2*n2 - 1; 2*n2; 2*n2 + 1; 2*n2 + 2; 2*n1 + 1; 2*n1 + 2], 1);
20. lp = (lmax - lmin)*x(ely, elx)^penal/(1 + (1 - x(ely, elx)^penal)*(lmax - lmin)/sdiag);
21. Uin = (lp + lmin)*inv((lp + lmin)*eye(8, 8) + KE)*Uout;
```

The sensitivity of the compliance with respect to the design variable  $\gamma_e = x(\text{ely}, \text{elx})$  is given by

```
22. dc(ely, elx) = -penal/x(ely, elx)*(lp + lp^2/sdiag)*(Uout - Uin)'*(Uout - Uin);
```

It can be seen that this is a relatively simple expression. Also when the problem involves physical non-linearities, this does not affect the complexity of the sensitivity analysis [9, 11].

Furthermore, the following line reflects the upper and lower bounds of the design variable in determining the design variable update. The lower bound  $\gamma_{\min}$  was set to be  $1.0 \times 10^{-8}$ .

```
42. xnew = max(1.0E-8, max(x - move, min(1., min(x + move, x.*(-dc./lmid).^0.5)))));
```

Finally, the compliance is calculated as

```
85. c = U'*F;
```

This code is available for downloading at [idealab.snu.ac.kr](http://idealab.snu.ac.kr) and can be used freely, provided that publications based on this code cite the present paper.

#### ACKNOWLEDGEMENTS

This research was supported by the National Creative Research Initiatives Program (Korea Science and Technology Foundation grant No. 2006-033) contracted through the Institute of Advanced Machinery Design at Seoul National University.

#### REFERENCES

1. Bendsøe MP, Sigmund O. *Topology Optimization Theory, Methods and Applications*. Springer: New York, 2003.
2. Bendsøe MP, Kikuchi N. Generating optimal topologies in structural design using a homogenization method. *Computer Methods in Applied Mechanics and Engineering* 1988; **71**:197–224.
3. Yoon GH, Kim YY. Element connectivity parameterization for topology optimization of geometrically nonlinear structures. *International Journal of Solids and Structures* 2005; **42**(7):1983–2009.
4. Bruns TE. Topology optimization by penalty (TOP) method. *Computer Methods in Applied Mechanics and Engineering* 2007; **196**:4430–4443.
5. Bruns TE, Tortorelli DA. An element removal and reintroduction strategy for the topology optimization of structures and compliant mechanisms. *International Journal for Numerical Methods in Engineering* 2003; **57**:1413–1430.

6. Yoon GH, Kim YY. The element connectivity parameterization formulation for the topology design optimization of multiphysics systems. *International Journal for Numerical Methods in Engineering* 2005; **64**(12):1649–1677.
7. Buhl T, Petersen CBW, Sigmund O. Stiffness design of geometrically nonlinear structures using topology optimization. *Structural and Multidisciplinary Optimization* 2000; **19**(2):93–104.
8. Cho SH, Jung HS. Design sensitivity analysis and topology optimization of displacement-loaded nonlinear structures. *Computer Methods in Applied Mechanics and Engineering* 2003; **192**:2539–2553.
9. Yoon GH, Kim YY. Topology optimization of material-nonlinear continuum structures by the element connectivity parameterization. *International Journal for Numerical Methods in Engineering* 2007; **69**:2196–2218.
10. Yoon GH, Joung YS, Kim YY. Optimal layout design for the three dimensional geometrical nonlinear structures using the element connectivity parameterization. *International Journal for Numerical Methods in Engineering* 2007; **69**:1278–1304.
11. Langelaar M, Yoon GH, Kim YY, Keulen FV. Topology optimization of shape memory alloy actuators using element connectivity parameterization. *Proceedings of the 6th World Congresses of Structural and Multidisciplinary Optimization*, Rio de Janeiro, Brazil, 2005.
12. Langelaar M, Keulen FV. Topology optimization of shell structures using element connectivity parameterization. *Proceedings of the 7th World Congresses of Structural and Multidisciplinary Optimization*, Seoul, Korea, 2007.
13. Woodbury M. Inverting modified matrices. *Memorandum Report 42*, Statistical Research Group, Princeton University, Princeton, NJ, 1950.
14. Sherman J, Morrison WJ. Adjustment of an inverse matrix corresponding to changes in the elements of a given column or a given row of the original matrix. *Annals of Mathematical Statistics* 1949; **20**:621.
15. Bathe KJ. *Finite Element Procedures*. Prentice-Hall: Englewood Cliffs, NJ, 1996.
16. Hassani B, Hinton E. *Homogenization and Structural Topology Optimization: Theory, Practice and Software*. Springer: New York, 1999.
17. Stolpe M, Svanberg K. An alternative interpolation scheme for minimum compliance topology optimization. *Structural and Multidisciplinary Optimization* 2001; **22**(2):116–124.
18. Sigmund O. A 99 line topology optimization code written in Matlab. *Structural and Multidisciplinary Optimization* 2001; **21**:120–127.
19. Jang GW, Jeong JH, Kim YY, Sheen D, Park C, Kim M. Checkerboard-free topology optimization using nonconforming finite elements. *International Journal for Numerical Methods in Engineering* 2003; **57**:1717–1735.